Temporal and spatial transients in turbulent boundary layer flow over an oscillating wall

Martin Skote[a,*]

[a] *School of Mechanical & Aerospace Engineering*
Nanyang Technological University
50 Nanyang Avenue, Singapore 639798

Abstract

Direct Numerical Simulations have been performed to study the effect of an oscillating segment of the wall on a turbulent boundary layer flow. Two different oscillation amplitudes with equal oscillation period have been used, which allows a direct comparison between a relatively weak and strong forcing of the flow. The weaker forcing results in 18% drag reduction while the stronger forcing, with twice the amplitude, yields 29% drag reduction. The downstream development of the drag reduction is compared with earlier simulations and experiments. In addition, a simulation with identical oscillation parameters as in previous numerical and experimental investigations allows for an estimation of the effect of the Reynolds number on the drag reduction.

Reductions in the Reynolds stresses and the important role that the edge of the Stokes layer has is explained.

An estimation of the idealized power consumption shows that a positive energy budget is only possible for the weaker wall velocity case.

Spatial and temporal transients are investigated and a transformation between spatial and temporal coordinates via a convection velocity is shown to facilitate a comparison between the two transients in a consistent manner. The streamwise shear exhibits a similar monotonic behavior in the spatial and temporal transients, while the non-monotinic temporal transient of the longitudinal Reynolds stress has no counterpart in the spatial development. Furthermore, the evolution in time of the spanwise Reynolds stress is very similar to previously reported channel flow data.

The instantaneous spanwise velocity profile (only averaged in the homogeneous spanwise direction) will for the first time be presented from a boundary layer over an oscillating wall, and comparisons with the analytical solution to the laminar Navier-Stokes equations show very good agreement.

Keywords: Direct Numerical Simulation, Turbulent Boundary Layer, Oscillating Wall, Drag Reduction

*Corresponding author
Email address: mskote@ntu.edu.sg. (Martin Skote)

1. Introduction

Controlling turbulence with the goal of reducing skin friction drag has for a long time been the subject of intense research. Many control strategies have been investigated in the past, both feedback-control techniques (Kasagi et al., 2009) and open-loop in the form of wall motion or body force (Karniadakis and Choi, 2003), with a varying degree of complicated structure of the control forcing. On the other hand, during the last 20 years a number of experimental and numerical studies have shown that a simple oscillation of the wall actually attenuates the turbulence significantly, and thus also reduces the viscous drag from the fluid flowing over the wall.

The first studies of turbulent flows over an oscillating wall were performed numerically using Direct Numerical Simulations (DNS) of channel flow by Jung et al. (1992). Inspiration for this work came from, among other investigations, earlier experiments and simulations of three-dimensional wall-bounded flows by Bradshaw and Pontikos (1985) and Moin et al. (1990). Later, Baron and Quadrio (1996) reported DNS results from a channel flow simulation with a spanwise oscillating wall and presented more details of the flow; the scaling of velocity profiles and Reynolds stresses, as well as the effect of oscillation on the turbulent energy budget.

Choi et al. (2002) performed DNS of both channel and pipe flow with oscillating walls and offer a phenomenological analysis of the mechanism of the drag reduction, related to high speed fluid penetrating beneath the low-speed streaks. Other attempts to model the mechanism of drag reduction in this context can be found in the investigations by Dhanak and Si (1999), Nikitin (2000) and Bandyopadhyay (2006).

Quadrio and Ricco (2003) conducted DNS of channel flow and analyzed the transient behavior in the first few cycles of wall oscillations. They noted that the spanwise velocity profile follows the analytical profile given by second Stokes problem. In another paper by Quadrio and Ricco (2004), much of the earlier DNS and experiments were reviewed and discrepancies regarding the resulting drag reduction were explained. The influence of the oscillation parameters, such as the amplitude and frequency, on the drag reduction was investigated. In addition, the energy savings possible to obtain were shown to be positive only for lower oscillation amplitudes.

The later paper by Xu and Huang (2005) offers an explanation of the drag reduction from the transport equations of the Reynolds stresses. In the more recent paper by Ricco and Quadrio (2008), a parameter based on the action of the oscillating Stokes layer, is shown to give a linear relation with the resulting drag reduction. The parameter will be discussed later in section 3.1.1.

Laadhari et al. (1994) were the first who confirmed that Jung's results also applied to the boundary layer flow. Since then, most of the experimental investigations have in fact been focused on the boundary layer. Other than the

investigations mentioned further below these experimental studies include the works of Choi (2002), Di Cicca et al. (2002) and Ricco (2004).

Experimental findings regarding the spatial development of the drag reduction can be found in the work of Choi et al. (1998), who reported a drag reduction upstream of the oscillating part of the wall. Also Ricco and Wu (2004) investigated the downstream development of the drag reduction but no upstream influence could be detected.

The reduction of Reynolds stresses in boundary layer flows over an oscillating wall has been quantified by Laadhari et al. (1994), Choi and Clayton (2001), Trujillo et al. (1997) and Ricco and Wu (2004). The exact numbers of the decrease in intensities will be discussed later in this paper (section 3.1.3), but the general trend is that the Reynolds shear stress reduces more than the streamwise and normal velocity fluctuations.

In the experiments conducted by Ricco and Wu (2004), the Reynolds number based on momentum thickness varied from 500 to 1500, and only a weak dependency of the Reynolds number on the drag reduction could be detected for a limited set of comparisons. On the other hand, the simulations performed by Choi et al. (2002) showed a strong dependency on the Reynolds number. In the present work, a simulation with exactly the same oscillation parameters as in Ricco and Wu (2004) is performed to confirm that the higher drag reduction (as compared with the experiments) found in the DNS can only be explained by the lower Reynolds number.

Lately, Yudhistira and Skote (2011) performed the only DNS, so far, on turbulent boundary layer over an oscillating wall, and the drag reduction development downstream followed that observed from experiments by Ricco and Wu (2004). The sensitivity on the Reynolds shear stress profiles on the turbulence statistics sampling time was investigated and some inconsistency in earlier experimental findings could be explained. The simulations presented here is a continuation of the work by Yudhistira and Skote (2011), and weaker wall oscillation amplitudes are chosen in order to investigate if a positive energy budget can be obtained.

The pipe flow has also been observed to exhibit drag reduction when the wall undergoes oscillations. First to study this type of flow was Choi and Graham (1998) who conducted experiments on oscillating pipe flow. The DNS performed by Quadrio and Sibilla (2000) showed evidence of the lateral displacement of low-speed streaks with respect to the streamwise vortices. They compared their results with the higher Reynolds number experimental data from Choi and Graham (1998).

Other investigations of oscillating pipe flow have been conducted by Nikitin (2000); Duggleby et al. (2007) (DNS) and Auteri et al. (2010) (experiment).

In addition, Large Eddy Simulation (LES) of compressible turbulent channel flow with spanwise wall oscillation has been performed by Fang and Lu (2010).

In the above mentioned investigations, the wall oscillation is imposed through a wall velocity (W) in the spanwise direction in the form of

$$W = W_m \sin(\omega t), \tag{1}$$

where W_m is the maximum wall velocity and ω is the angular frequency of the wall oscillation, which is related to the period (T) through $\omega = 2\pi/T$. The wall oscillation in the experiments is often implemented via the maximum wall displacement D_m, which is related to maximum wall velocity through

$$D_m = W_m T/\pi. \tag{2}$$

The oscillation in time may not be practical to implement in an engineering application which has recently lead researchers (Viotti et al., 2009; Quadrio et al., 2009; Quadrio and Ricco, 2011; Skote, 2011) to consider a steady variation in the streamwise direction along the plate instead of a time-dependent forcing. In this case, the wall velocity (W) is imposed in the form of

$$W = W_m \sin(\kappa x), \tag{3}$$

where κ is the wavenumber of the spatial oscillation, which is related to the wavelength (λ_x) through $\kappa = 2\pi/\lambda_x$.

The work so far on this type of spatial oscillation has solely been performed using DNS of channel flow by Viotti et al. (2009) and boundary layer flow by Skote (2011). Quadrio et al. (2009) have studied (through DNS) the combination of spatial and temporal wall oscillation (stream-wise travelling waves) in a channel flow. However, only marginal improvement on the drag reduction (compared to the stationary forcing) was obtained. The theoretical and numerical studies were recently further developed by Quadrio and Ricco (2011).

In the present paper simulations of turbulent boundary layers subjected to a forcing of form (1) will be presented. In total, four simulations have been performed; the unmanipulated (non-oscillating) turbulent boundary layer, a boundary layer flowing over an oscillating wall with two different wall velocities (but with equal oscillation period), while the last simulation is conducted with identical oscillation parameters as an earlier channel flow simulation by Quadrio and Ricco (2004) and boundary layer experiment by Ricco and Wu (2004). Our results are compared with other investigations; both with experiments and DNS, as well as for both boundary layer flow and channel flow. In addition, the spatial and temporal transients will be investigated as well as the statistically stationary flow. Furthermore, the spanwise flow is shown to be described by the laminar equations.

The paper is organized as follows. In section 2 the numerical method and simulation related issues are discussed. The results are presented in section 3, which is divided into three parts. In the first part (3.1) the general flow features are investigated with respect to drag reduction, Reynolds number dependency, turbulence statistics and energy budget. In the second part (3.2) the temporal and spatial transients are compared. The results section is concluded with a presentation of the instantaneous velocity profiles (3.3). Lastly, conclusions are drawn in section 4.

2. Numerical method and simulation parameters

The numerical code and grid are the same as in the previous simulation of an oscillating turbulent boundary layer reported by Yudhistira and Skote (2011), who also showed that the grid is sufficiently fine. The code was developed at KTH, Stockholm (Chevalier et al., 2007). A recent simulation of a turbulent boundary layer at $Re_\Theta = 2500$ was performed by Schlatter et al. (2009) with results in excellent agreement with experimental data at the same Reynolds number. An outline of the numerical scheme is presented in section 2.1, the various parameters used and the resolution are presented next in section 2.2, where also the implementation of the wall motion is presented.

2.1. Numerical Scheme

A pseudo-spectral method is employed, with Fourier discretization used in the streamwise and spanwise directions, and Chebyshev polynomials in the wall-normal direction. The simulations start with a laminar boundary layer at the inflow which is triggered to transition by a random volume force near the wall. Details can be found in Yudhistira and Skote (2011).

A fringe region is added at the end of the computational domain to enable simulations of spatially developing flows. In this region the flow is forced from the outflow of the physical domain to the inflow. In this way the physical domain and the fringe region together satisfy periodic boundary conditions. The implementation is done by adding a volume force

$$F_i = \lambda(x)(\widetilde{u}_i - u_i) \tag{4}$$

to the Navier-Stokes equations,

$$\frac{\partial u_i}{\partial t} + u_j \frac{\partial u_i}{\partial x_j} = -\frac{1}{\rho}\frac{\partial p}{\partial x_i} + \nu \frac{\partial^2 u_i}{\partial x_j^2} + F_i \tag{5}$$

The force F_i acts only in the fringe region. $\widetilde{u}_i$ is the laminar inflow velocity profile the solution u_i is forced to and $\lambda(x)$ is the strength of the forcing. The form of the fringe function is designed to have minimal upstream influence and is given by

$$\lambda(x) = \lambda_{max} f(x) \tag{6}$$

with

$$f(x) = S\left(\frac{x - x_{start}}{\Delta x_{rise}}\right) - S\left(\frac{x - x_{end}}{\Delta x_{fall}} + 1\right). \tag{7}$$

Here λ_{max} is the maximum strength of the fringe, x_{start} and x_{end} denotes the spatial extent of the region where the fringe is non-zero, Δx_{rise} and Δx_{fall} are the rise and fall distance of the fringe function respectively. $S(x)$ is a continuous step function that rises from zero for negative x to unity for $x \geq 1$. The expression of $S(x)$, which has the advantage of having continuous derivatives of all orders is,

$$S(x) = \begin{cases} 0, & x \leq 0, \\ 1/(1 + e^{(1/(x-1)+1/x)}), & 0 < x < 1, \\ 1, & x \geq 1. \end{cases} \tag{8}$$

The function $f(x)$ is also utilized in the implementation of the wall oscillation described in section 2.2 below.

The time integration is performed using a third-order Runge-Kutta-scheme for the non-linear terms and a second-order Crank-Nicolson method for the linear terms. A 3/2-rule is applied to remove aliasing errors from the evaluation of the non-linear terms when calculating FFTs in the wall parallel plane.

2.2. Numerical parameters

All quantities are non-dimensionalized by the free-stream velocity (U) and the displacement thickness (δ^*) at the starting position of the simulation ($x = 0$), where the flow is laminar. The Reynolds number is set by specifying $Re_{\delta^*} = U\delta^*/\nu$ at $x = 0$. In all the simulations presented here, $Re_{\delta^*} = 450$. The computational box is 600 in simulation length units (δ^*) long (including 100 units for the fringe), 30 units high and 34 units wide.

As the fringe starts at $x = 500$, only results up to $x = 470$ will be utilized to avoid any upstream influence of the fringe. The transition region is roughly between $x = 5$ and $x = 150$. Thus, the region of a fully developed turbulent boundary layer, free from any influence of the numerical method, is $x = 150 - 470$. The Reynolds number based on the momentum thickness (Re_θ) is varying between 387 and 725 in this region for the unmanipulated (reference) boundary layer. In inner scaling (based on the friction velocity at $x = 250$), the region amounts to about 7200 wall units.

The code has been modified to allow for an oscillating spanwise wall-velocity, and the implementation is very similar to the one used by Yudhistira and Skote (2011), except that no ramp-up time in the formula for the wall velocity in included. The wall oscillation is applied in the spanwise direction at a particular region in streamwise direction. Therefore, a profile function $f(x)$ is utilized to serve as a filter to select the domain where the oscillation takes place.

The form of this boundary condition is given by

$$w|_{y=0} = W_m f(x) \sin[\omega(t - t_{start})] \tag{9}$$

where $f(x)$ is the same profile function as used for fringe region, see equation (7), with x_{start}, x_{end}, x_{rise} and x_{fall} set to 250, 483, 10 and 10 respectively. The parameter ω is the angular frequency of the wall oscillation, which is related to the period through $\omega = 2\pi/T$. The streamwise variation of the wall velocity is illustrated in Figure 1 at the instant of maximum positive (solid line) and maximum negative (dashed line) wall velocity.

The resolution used for the simulations were 800 modes in streamwise direction, 201 modes in wall-normal direction, and 144 modes in the spanwise direction. This grid size result in a spatial resolution of $\Delta X^+ \times \Delta Z^+ \times \Delta Y^+_{min} =$

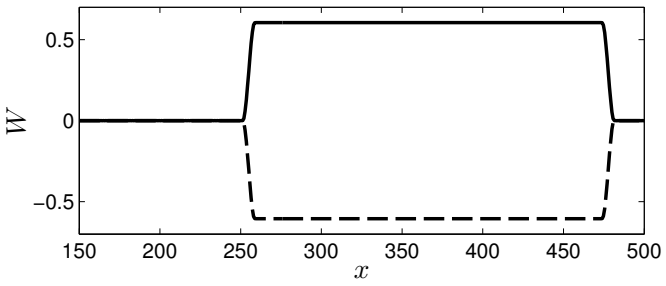

Figure 1: Downstream variation of the wall velocity. (—) at maximum positive wall velocity; (− −) at maximum negative wall velocity.

$16 \times 5.1 \times 0.04$. Note that unless otherwise stated, the + superscript indicates that the quantity is made non-dimensional with the friction velocity of the unmanipulated boundary layer (the reference case), denoted u_τ^0, and the kinematic viscosity (ν).

The sampling time for the reference case was 6000 in time units (δ^*/U), started only after a stationary flow (in the statistical sense) was reached. In the cases with wall forcing, the total sampling time was 8000 after an initial simulation time of 6000 with oscillations.

In the simulations presented here the angular frequency (ω) of the wall oscillation is first set to 0.0545 while two different values for the maximum wall velocity (W_m) were used; 0.3025 and 0.605 respectively, which in wall units corresponds to $T^+ = 132$ and $W_m^+ = 6$ and $W_m^+ = 12$, based on u_τ^0 where the wall forcing starts ($x = 250$). These parameters were chosen in order to examine the effect of wall velocity on the drag reduction while applying an optimal value of the oscillation period. In the following the lower amplitude case will be referred to as case 1 while the larger amplitude simulations is denoted case 2.

In order for a direct comparison with earlier DNS and experiments, another simulation was performed with $W_m^+ = 11.3$ and $T^+ = 67$, which hereafter will be denoted case 3.

The total length of applied wall motion is 5380 in wall units, and the Reynolds number at the onset of oscillation is $Re_\Theta = 503$, for all simulations.

3. Results

This section starts with a presentation of the general flow features (3.1), which follows by an investigation of the transient behavior of the flow (3.2), and concludes with a presentation of the instantaneous velocity profiles (3.3).

3.1. General flow features

In the previous simulation by Yudhistira and Skote (2011) it was shown that the most sensitive statistical quantity with respect to the length of sampling time is the Reynolds shear stress. Thus, as a measure of the grade of

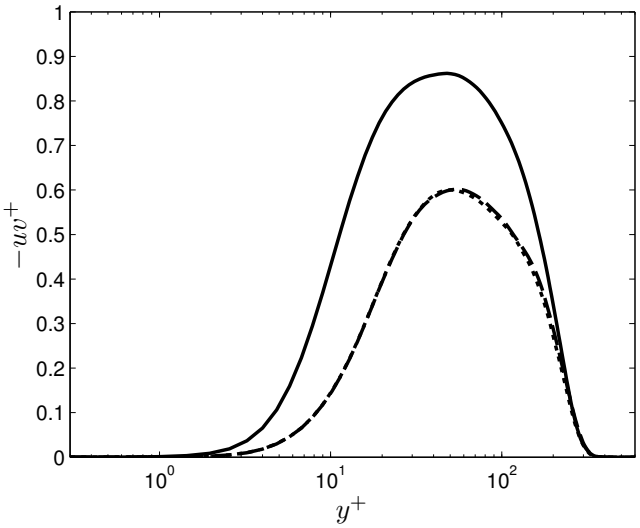

Figure 2: Reynolds shear stress profiles at $x = 450$. (—) Reference case; (− −) Statistics from $t = 6000 - 10000$; $(\cdots)$ Statistics from $t = 10000 - 14000$; The profiles are scaled with u_τ^0 at $x = 450$.

convergence of the turbulence statistics the Reynolds shear stress from two different time interval are shown in Figure 2. Only small variation can be detected in contrast to the large deviations found in Yudhistira and Skote (2011) when shorter intervals were chosen. Hence, the turbulence statistics can be considered stationary and will in the following be taken from the interval $t = 6000 - 14000$, which corresponds to $\Delta t^+ = 9145$ in wall units.

In the three sections that follow, the general observations regarding drag reduction, Reynold number dependence, turbulence statistics and energy saving budgets will be discussed.

3.1.1. Drag Reduction

The friction coefficient is defined as

$$C_f = 2\left(\frac{u_\tau}{U_\infty}\right)^2, \tag{10}$$

where the friction velocity u_τ is calculated from the mean streamwise velocity gradient at the wall:

$$u_\tau \equiv \sqrt{\nu \left.\frac{\partial u}{\partial y}\right|_{y=0}} \tag{11}$$

The resulting drag reduction (DR) is calculated from

$$\mathrm{DR}(\%) = 100\frac{C_f^0 - C_f}{C_f^0}, \tag{12}$$

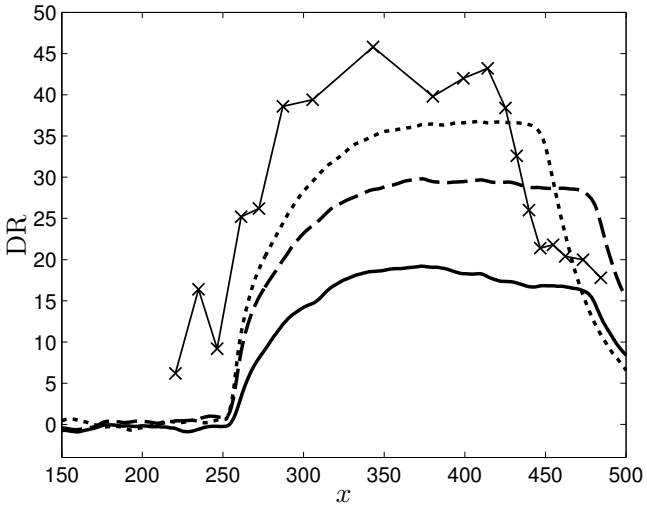

Figure 3: Downstream development of the drag reduction. (—) case 1; (− −) case 2; (· · ·) $W_m^+ = 17$ ($T^+ = 118$) from Yudhistira and Skote (2011); − × − $W_m^+ = 7.1$ ($T^+ = 154$) from Choi et al. (1998).

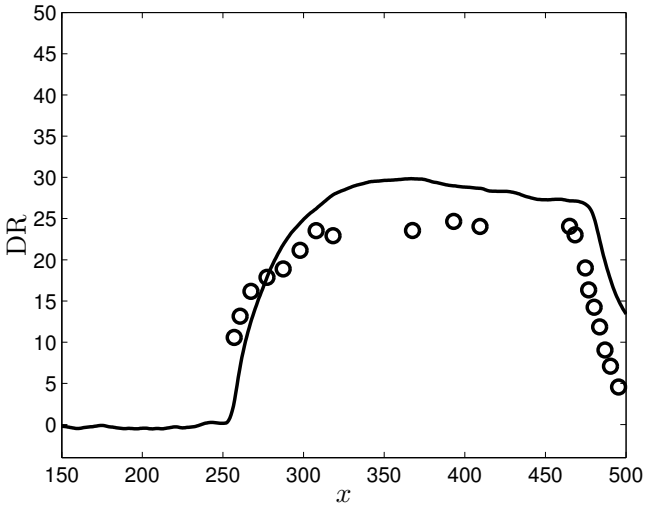

Figure 4: Downstream development of the drag reduction. (—) case 3; ◯ $W_m^+ = 11.3$ ($T^+ = 67$) from Ricco and Wu (2004).

where C_f^0 is the skin friction of the reference case.

The downstream development of the DR is shown in Figure 3 for case 1 (represented by the solid line) and case 2 (dashed line). The downstream development of the DR is similar to the previous temporal oscillating case (Yudhistira and Skote, 2011) with a higher wall velocity of $W_m^+ = 17$ (dotted line in Figure 3). Observe that the wall velocity W_m^+ was determined to be 18 in the original work (Yudhistira and Skote, 2011) based on u_τ^0 at the end of the fully turbulent boundary layer at $x = 470$. However, in order to have consistent scaling, the value at the onset of oscillation ($x = 250$) is chosen in the present work. Hence the value $W_m^+ = 17$ used herein. Similarly, the period T^+ which was calculated as 100 in Yudhistira and Skote (2011) is changed to 118 when using u_τ^0 at the onset of oscillation. Note that the wall forcing ends at $x = 450$ in this case and hence the DR reduces from that point, whereas the end-point is located at $x = 482.7$ for cases 1 and 2.

The experimental data from Choi et al. (1998) are also included in Figure 3 as symbols ($\times$) and a thin line. Note that the downstream coordinate is scaled such that the experimental data can be compared with the DNS, and the oscillation for all cases start at $x = 250$. Thus, the three first data points from Choi et al. (1998) are upstream of the onset of oscillation and a DR of more than 15% was observed there. This upstream DR was not detected neither in the experiments by Ricco and Wu (2004) nor in the present or earlier DNS.

When calculating the W_m^+ and T^+ for the experiment conducted by Choi et al. (1998) the friction velocity u_τ^0 needs to be estimated by utilizing the relation which was shown by Schlatter and Orlu (2010) to be valid for similar Reynolds numbers,

$$C_f = 2(u_\tau/U_\infty)^2 = 0.024 Re_\Theta^{-0.25} \tag{13}$$

which yields $u_\tau^0 = 0.11$. From the oscillation parameters given in Choi et al. (1998) we can deduct that $W_m^+ = 7.1$ and $T^+ = 154$. The DR reaches values up to 45% as shown in Figure 3. This value is much higher than what other experiments and DNS investigations have obtained for similar oscillation parameters (see below). The oscillation ends at the position $x = 435$ and thus the six last data points are located downstream of the oscillation. The high value of the DR and the behavior upstream and downstream of the oscillating plate give the impression that the whole DR curve is shifted upward with about 15% (which would give a maximum DR of around 30% in better agreement with the theoretical expression and other DNS and experiments as presented below).

The downstream development of the DR for case 3 is shown in Figure 4 and compared with the experiments by Ricco and Wu (2004), included in Figure 4 as symbols ($\bigcirc$). The oscillation parameters are identical for these two cases ($W_m^+ = 11.3$ and $T^+ = 67$) and it will be concluded in section 3.1.2 that the discrepancy in DR is due to the difference in Reynolds number between the DNS and experiment.

Returning to cases 1 and 2 (Figure 3) with equal period ($T^+ = 132$), we observe that the maximum DR for case 1 ($W_m^+ = 6$) and case 2 ($W_m^+ = 12$) is

DNS boundary layer				DNS channel flow[a]			
W_m^+	T^+	DR	Eq. 14	W_m^+	T^+	DR	Eq. 14
6	132	18.0	19.4	6	125	22.1	19.4
12	132	29.4	30.5	12	125	32.5	30.5
17[b]	118	36.5	36.1	18	100	39.1	36.8

[a] Data taken from Quadrio and Ricco (2004)

[b] Data taken from Yudhistira and Skote (2011)

Table 1: Comparison of DR between present cases 1 and 2, and earlier DNSs of boundary layer flow and channel flow, and Equation (14).

19.2% and 29.8% respectively, which is substanially lower than the corresponding DR for the earlier case ($W_m^+ = 17$) which is 36.8%. For the present cases the period was set to $T^+ = 132$ in order to obtain a near optimum DR. When calculating a mean DR by integrating over a length of relatively constant DR, in this case $x = 366 - 450$, we get 18.0% and 29.4% for case 1 and 2 respectively, compared to 36.5% for the earlier case.

Ricco and Quadrio (2008) have suggested a parameter S that varies linearly with the drag reduction according to

$$\mathrm{DR}(\%) = S_1 S + S_2, \tag{14}$$

where $S_1 = 135.11$ and $S_2 = -0.85$ are two constants determined by fitting the linear expression to experimental and numerical drag reduction data. The expression for dimensionless drag reduction scaling parameter S is given by:

$$S = \frac{a_m^+ l_w^+}{W_m^+} = 2\sqrt{\frac{\pi}{T^+}} \ln\left(\frac{W_m^+}{W_{th}^+}\right) \exp\left(-l_a^+ \sqrt{\pi/T^+}\right). \tag{15}$$

The + superscript denotes variables in inner (wall) scaling.

Here a_m^+ and l_w^+ represent the scaled maximum acceleration of the Stokes layer, and the scaled wall-normal distance respectively, while W_m^+ is the scaled maximum wall velocity. The scaled period of wall oscillation is given by T^+, while W_{th}^+ denotes threshold spanwise velocity, and l_a^+ is scaled wall-normal distance at which a_m^+ is computed. The parameters l_a^+ and W_{th}^+ have been determined by maximizing the correlation coefficient between the drag reduction data and S. The value of the parameters given in Ricco and Quadrio (2008) are: $l_a^+ = 6.2$ and $W_{th}^+ = 1.7$.

Equation (14) yields 19.4% and 30.5% for case 1 and 2 respectively, which is close to the DNS results of 18.0% and 29.4% respectively. Remember that the DR has been computed by averaging over the $x-$direction ($x = 366 - 450$) with approximately constant DR. In fact, the DR from present DNS compares better with Equation (14) than values from channel flow with similar parameters. The results regarding DR are summarized in Table 1 where the present (cases 1 and 2) and earlier DNS results are summarized and compared to Equation (14). In the last row of Table 1, the oscillation period for the boundary layer DNS is

$T^+ = 118$ while for the channel flow DNS $T^+ = 100$, which may seem to be a large difference. However, the data from Quadrio and Ricco (2004) show that for a fixed amplitude of $W_m^+ = 18$, applying $T^+ = 100$ and $T^+ = 125$ yields a DR of 39.1% and 39.3% respectively, which indicates that at high values of W_m^+, the DR is relatively insensitive to the value of the oscillation period.

The lower values of the DR in the present simulations (case 1 and 2) compared to the channel flow cases (see Table 1) are not due to the slightly larger values of the period used in the present boundary layer simulations (since the DR is not sensitive to the period at these values of the oscillation parameters, see Quadrio and Ricco 2004, Figure 1), but is an effect of either geometry or Reynolds number. The analysis in section 3.1.2 below will indicate, by comparing the present data with earlier channel flow simulations and boundary layer experiments, that a reasonable conclusion is that the Reynolds number variation is the cause behind the DR discrepancy, and not the flow geometry.

As noted in Table 1, the boundary layer DR is consistently lower than channel flow data, which can also be seen when comparing the experimental data of Ricco and Wu (2004) with $W_m^+ = 11.3$ and $T^+ = 67$, which resulted in a DR of 23%, while the channel flow DNS by Quadrio and Ricco (2004) gave 31.2% with exactly the same oscillation parameters. The present simulation (case 3) with identical parameters resulted in a DR of 28.6%. See Table 2 for a comparison of the studies above together with Equation (14) which yields 28.1% for these parameters. Note that the difference in DR between the experimental and numerical boundary layer is larger than between the numerical channel and boundary layer. Again, the analysis in section 3.1.2 below will show that the variation of DR is explained by the different Reynolds numbers used in the studies.

On the other hand, equation (14) does not explicitly depend on Reynolds number which is consistent with (and motivated by) the experimental work by Ricco and Wu (2004). In their investigation, only a weak dependency of the Reynolds number on the drag reduction could be detected for a limited set of comparisons from $Re_\Theta = 500$, 950 and 1400. In contrast, the simulations performed by Choi et al. (2002) showed a strong dependency on the Reynolds number. In order to determine what causes this discrepancy there is a need to investigate the effect of Reynolds number, which is done in the next section, where the data in Table 1 and 2 will be analyzed with respect to the Reynolds number dependence instead of the geometry variation.

3.1.2. Reynolds number dependency

In order to conclude that the Reynolds number indeed affects the DR, we utilize case 3, which is a simulation that was performed at the same Reynolds number as case 1 and case 2 ($Re_\Theta = 503$) but with $W_m^+ = 11.3$ and $T^+ = 67$. The resulting DR is very close to case 2 (compare Figures 3 and 4) and confirm earlier conclusions (see Ricco and Quadrio, 2008, Figure 6) that for $W_m^+ \approx 12$ an approximately constant DR is obtained, independently on T^+ when $T^+ \gtrsim 65$. However, as noted earlier, the DR from case 3 is much larger than the DR from the experimental boundary layer, and slightly lower compared to the channel

DNS channel[a]	DNS boundary layer	Experiment boundary layer[b]	Eq. 14
$Re_\tau = 200$ ($Re_\Theta = 375$)	$Re_\Theta = 503$	$Re_\Theta = 1400$	
31.2	28.6	23	28.1

[a] Data taken from Quadrio and Ricco (2004)
[b] Data taken from Ricco and Wu (2004)

Table 2: Comparison of DR between boundary layer flow and channel flow at various Reynolds numbers for $W_m^+ = 11.3$ and $T^+ = 67$. (Case 3 in the present work.)

flow DNS. Refer to Table 2 for a summary of the three different DR values for equal oscillation parameters.

The differences in DR from present DNS of boundary layer flow and earlier DNS of channel flow can be explained with the Reynolds number variation between the cases. Furthermore, the experiment at higher Reynolds number of the boundary layer flow and the resulting low value of DR also agree with this concept. In order to strengthen the arguments, the channel flow DNS by Choi et al. (2002) is also utilized. Of interest here is the general trend of the DR with respect to the Reynolds number when various sets of oscillation parameters are used. The conclusion from the investigation by Ricco and Quadrio (2008) was that the Reynolds number dependency is weaker for lower values of the oscillation period. In the present analysis we do not attempt to elaborate on the relation between Reynolds number dependency and oscillation parameters due to the lack of data.

The DR in tables 1 and 2 are now presented versus Reynolds number in the same graph in Figure 5. In order to translate from Re_τ to Re_Θ we use the relation derived by Ricco and Quadrio (2008) for similar Reynolds numbers:

$$Re_\Theta = \left(\frac{Re_\tau}{1.118} \right)^{1.143}. \tag{16}$$

Included in Figure 5 are some of the channel flow DNS at different Reynolds numbers produced by Choi et al. (2002). The data sets are for $W_m^+ = 5$, $T^+ = 50$ and $W_m^+ = 10$, $T^+ = 50$ and $W_m^+ = 20$, $T^+ = 100$ respectively. For these three variations of the oscillation parameters, simulations at three Reynolds numbers were performed, namely $Re_\tau = 100$, 200 and 400, which corresponds (according to Equation 16) to $Re_\Theta = 170$, 375, 829.

The general trend for all the data is that the DR decreases for increasing Reynolds numbers. Another conclusive observation is that the DR profiles are levelling out for higher Reynolds numbers. This is in agreement with the conclusion by Ricco and Quadrio (2008) who also speculated if there exists a Reynolds number (unique for each set oscillation parameters) above which there is no change in DR.

The two data points collapsing in Figure 5 are from the channel flow simulations at $Re_\tau = 200$ by Quadrio and Ricco (2004) (with $W_m^+ = 18$, $T^+ = 100$) and Choi et al. (2002) (with $W_m^+ = 20$, $T^+ = 100$). The nearly collapsing data

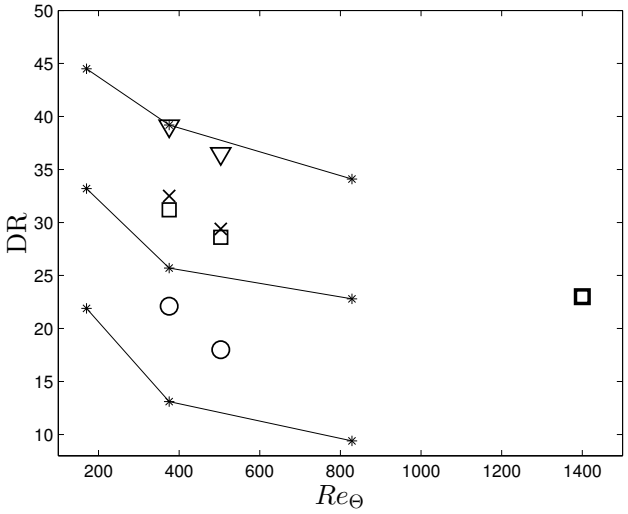

Figure 5: Drag reduction versus Reynolds number (Re_Θ). ◯ and × represent case 1 and 2, and the corresponding channel flow data from Quadrio and Ricco (2004); ▽ is the third case in Table 1 with data from Yudhistira and Skote (2011) and Quadrio and Ricco (2004); □ is the case with $W_m^+ = 11.3$ and $T^+ = 67$, the thick symbol represent the experiment by Ricco and Wu (2004); ∗ with connecting lines are the data taken from channel flow DNS by Choi et al. (2002).

(symbols × and □ in Figure 5) are cases 2 and 3 which have similar amplitudes but with the period of case 2 almost double that of case 3 ($T^+ = 132$ and $T^+ = 67$ respectively). Note that the data at $Re_\Theta = 503$ are from the present simulation, while the ones at $Re_\Theta = 375$ are taken from Quadrio and Ricco (2004).

The reason why Ricco and Wu (2004) did not find any dependency on the Reynolds number when comparing the DR for $Re_\Theta = 500$ and 950, and 950 and 1400, respectively, might be that the comparison was made between cases with relatively large Reynolds numbers, while the simulations by Choi et al. (2002) are performed at low Reynolds numbers, for which the influence is large on the DR even for a small variations. Another reason mentioned in Ricco and Quadrio (2008) is that the Reynolds number dependency is weaker for low values of the oscillation period which were used in the experiments by Ricco and Wu (2004).

3.1.3. Turbulence Statistics

The longitudinal (rms-value), normal (rms-value), and shear Reynolds stresses at $x = 450$, scaled with u_τ^0, are shown in Figure 6. Profiles from cases 1 and 2 are shown, together with the reference profiles (the higher curves). The reductions for case 1 and case 2 in maximum u_{rms}^+ is 15% and 27% respectively, and 11% for case 1 and 20 % for case 2 in maximum v_{rms}^+. For the Reynolds shear stress ($\overline{uv}^+$) the reductions are larger; 16% and 30% respectively. The effect of the wall oscillation on the Reynolds stresses follows that observed by

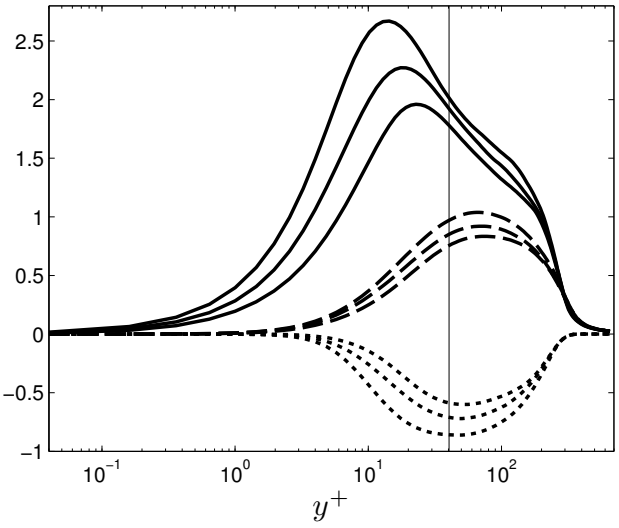

Figure 6: Reynolds stresses at $x = 450$. (—) u^+_{rms}; (− −) v^+_{rms}; (· · ·) $\overline{uv}^+$; the higher curves are the unmanipulated boundary layer; the lower curves are for the oscillating wall cases, scaled with u^0_τ. The vertical line at $y^+ = \delta^+_s$.

other researchers. Compared to the experimental data in Laadhari et al. (1994) who reported 45%, 34% and 50% for the three quantities, the present values are low, although the ratio between the different values seems to agree. On the other hand, values reported by Trujillo et al. (1997) was 15%, 25% and $20\% - 40\%$ (depending on whether the peak-to-peak values were used). Ricco and Wu (2004) reported lower values at 14% for u^+_{rms} and 25% for $-\overline{uv}^+$ for two experiments with different W^+_m (9 and 18) and T^+ (83 and 42), but equal $D^+_m = 240$. Even though the values of the Reynolds stress reduction were equal in the two experiments by Ricco and Wu (2004), they lead to different drag reduction of 25% and 32% respectively.

The Reynolds stresses in the present simulations behave, not surprisingly, in the same way as reported from the previous case by Yudhistira and Skote (2011) (with $W^+_m = 17$). However, the maximum reduces less than the corresponding values from the previous case, which were 33%, 22% and 40% for longitudinal (rms-value), normal (rms-value), and shear Reynolds stresses respectively.

A line is added in Figure 6 which corresponds to $y^+ = 40.7$, which marks the edge of the Stokes layer, denoted depth of penetration in Schlichting (1979). This edge is calculated from the region dominated by the laminar Stokes layer, which is below $y^+ < \delta^+_s = \sqrt{4\pi T^+}$, which in this case yields $\delta^+_s = 40.7$. In section 3.2.1 the Stokes layer will be further discussed.

Now, when comparing the position of the maximums of the Reynolds stresses it may be noted that for the longitudinal Reynolds stress (u_{rms}), the peak is located below the edge, while the normal and shear stresses are positioned above. Thus, it might be suspected that the maximum in u_{rms} is affected more by the

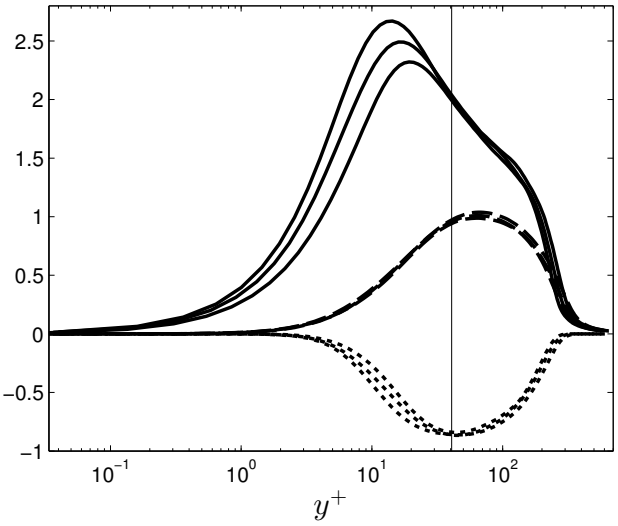

Figure 7: Reynolds stresses at $x = 450$. (—) u^+_{rms}; (− −) v^+_{rms}; (· · ·) $\overline{uv}^+$; the higher curves are the unmanipulated boundary layer; the lower curves are for the oscillating wall cases, scaled with actual u_τ. The vertical line at $y^+ = \delta^+_s$.

oscillating Stokes layer than the normal and shear stresses. To detect this, the stresses in Figure 6 are scaled with the actual friction velocity u_τ and plotted in Figure 7. In agreement with the reasoning above, the peak in u_{rms} is greatly affected while normal and shear stress peaks exhibits a much less reduction.

In Figure 8 the correlation coefficient

$$R_{uv} = \frac{\overline{uv}}{u_{rms} v_{rms}}, \tag{17}$$

for the reference case is shown together with case 1 and case 2. Here, the evidence is clear that the turbulence is greatly affected by the wall oscillation only in the region below $\delta^+_s = 40.7$. This position is exactly where the difference between the correlation coefficient starts to deviate, see Figure 8. In addition, the R_{uv} is lower near the wall for larger wall oscillation, which indicates that the Reynolds shear stress is more affected by the oscillation than the single-component longitudinal and normal *rms*-values. Similar findings were reported from the investigation by Quadrio and Ricco (2011).

3.1.4. Energy Saving

The energy saving due to DR is compared to the energy required to oscillate the wall by estimating the idealized power consumption, following the derivation by Quadrio and Ricco (2004), and extended to boundary layer flow. The percentage saved power $P_{sav}(\%)$ (in terms of the friction power of the reference flow) is equal to the percentage of friction DR (Equation 12), and integrated over a distance with approximately constant DR (in this case $x = 366 - 450$).

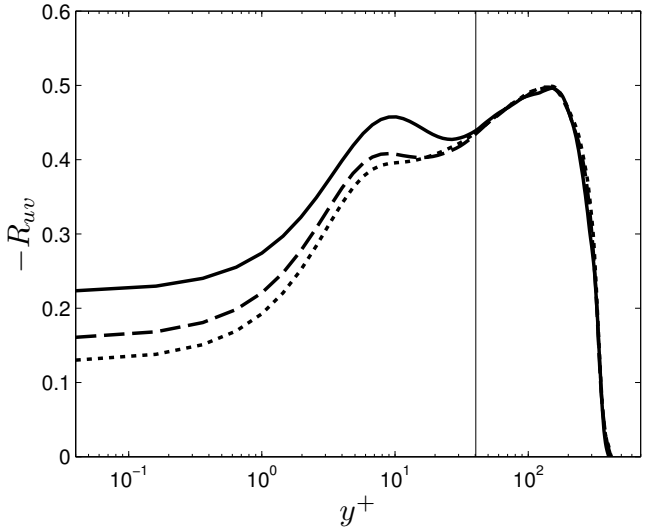

Figure 8: Correlation coefficient scaled with u_τ^0 at $x = 450$. (—) Reference case; (− −) case 1; (· · ·) case 2. The vertical line at $y^+ = \delta_s^+$.

Thus, the percentage saved power can be written as,

$$P_{sav}(\%) = \frac{1}{L}\int_{x_i}^{x_f} DR(\%)\mathrm{d}x \tag{18}$$

with $x_i = 366$, $x_f = 450$ and $L = x_f - x_i$.

The required (to oscillate the wall) percentage power $P_{req}(\%)$ is similarly defined in terms of the friction power of the reference flow and may be written as:

$$\begin{aligned} P_{req}(\%) &= 100\frac{1}{L}\int_{x_i}^{x_f}\frac{1}{T}\int_{t_i}^{t_f}\nu\frac{\partial w}{\partial y}\bigg|_{y=0}^{\mathrm{osc}} W\mathrm{d}t\mathrm{d}x \\ &\quad \Big/ \frac{1}{L}\int_{x_i}^{x_f}\frac{1}{T}\int_{t_i}^{t_f}\nu\frac{\partial u}{\partial y}\bigg|_{y=0}^{\mathrm{ref}} U\mathrm{d}t\mathrm{d}x, \end{aligned} \tag{19}$$

where *osc* and *ref* refer to the oscillating and reference case respectively. In addition to the integrations over t and x, an integration in the spanwise direction (z) is required, but is omitted in the formula since the flow is homogeneous in that direction. Furthermore, a factor equal to density times area is omitted in both numerator and denominator.

Since we calculate the energy after the initial transient has disappeared, the classical solution to the Stokes problem can be used in the first part of the formula (19) with $t_i = 0$ and $t_f = T$, and the statistical averaged value is used in the second part. That the laminar solution (Stokes problem) is valid here

DNS boundary layer				DNS channel flow[a]			
W_m^+	P_{sav}	P_{req}	P_{net}	W_m^+	P_{sav}	P_{req}	P_{net}
6	18.0	-15.2	2.85	6	22.1	-17.7	4.4
12	29.4	-60.8	-31.5	12	32.5	-71.4	-38.9
17[b]	36.5	-133	-96.5	18	39.1	-180.7	-141.6
11.3	28.6	-75.6	-47.0	11.3	31.2	-87.8	-56.6

[a] Data taken from Quadrio and Ricco (2004)
[b] Data taken from Yudhistira and Skote (2011)

Table 3: Comparison of percentage power saving and required power for the oscillations between boundary layer flow and channel flow.

even though the flow is turbulent will be shown in section 3.2.1. The required energy for moving the wall does not change downstream which means that the spatial integration can be omitted in the first part of formula (19), while it reduces to taking the spatial average of the wall shear stress in the second part. For the spatial integration, a section with constant DR is chosen; hence we set $x_i = 366$ and $x_f = 450$ (referring to Figure 3) and denote the distance between the two positions as L. With these observations formula (19) yields,

$$P_{req}(\%) = 100\frac{W_m^2}{2}\sqrt{\nu\omega/2}\Big/\frac{U}{L}\int_{x_i}^{x_f}(u_\tau^0)^2\mathrm{d}x. \tag{20}$$

The net percentage power saving is defined as $P_{net} = P_{sav} + P_{req}$ and is calculated for all three simulations in the present investigation, together with the earlier simulation by Yudhistira and Skote (2011). If P_{net} is negative it means that the power needed to drive the wall in the spanwise direction is greater than the power saved by streamwise DR.

The required power for the oscillations are compared with the energy saving in Table 3. The results are consistent with the channel flow simulations by Quadrio and Ricco (2004) which are included in the table for reference.

One important observation from these results is that the net energy saving is larger for lower values of oscillation amplitude, which means that the DR is sufficiently large at lower amplitudes while P_{req} is substantially lower, yielding a positive net energy saving.

3.2. Temporal and spatial transients

This section is devoted to the transient behavior and the initial response of the turbulent boundary layer to the oscillating wall. In the first part (3.2.1) the temporal transient of the spanwise shear (or equivalently, the normal gradient of the spanwise velocity), which is shown to follow closely the solution to the laminar equations. The streamwise shear is investigated in the second part (3.2.2), where both spatial and temporal transients are investigated and compared. Lastly, in section (3.2.3) the spatial and temporal transients of the Reynolds stresses are compared by investigating profiles from various time instances and spatial positions.

The main idea in sections (3.2.2) and (3.2.3), is that the spatial transients seen in the DR (Figure 3) have a close relation to the temporal transients already observed in channel flow simulations (Quadrio and Ricco, 2003). For the purpose of comparison, the temporal transients are calculated by averaging over a region where the flow is spatially constant ($x = 366 - 450$). The transient behavior is considered from the time the oscillations start ($t = 0$) until no transients can be seen at around $t = 4T \approx 520$. Likewise, the spatial transients are obtained by analyzing the downstream region between the onset of oscillation ($x = 250$) until the flow is fully adjusted at $x \approx 366$, for the statistically stationary flow from $t = 6000 - 14000$.

There is of course a spatial development in the downstream direction, but the variation is too small to draw any conclusions about the Reynolds number dependency.

3.2.1. Spanwise shear

Since the wall velocity starts without any ramp-up the flow is locally similar to the Stokes second problem (the laminar flow produced by a oscillating plate moving according to Equation (1)). The steady periodic solution can be expressed as (Schlichting, 1979),

$$w(y,t) = W_m \exp(-\eta)\sin(\omega t - \eta) \tag{21}$$

where $\eta = y\sqrt{\omega/2\nu}$. The profile (21) is not an exact expression of w in this case, since the spatially developing boundary layer has been approximated with a parallel flow (hence, the normal velocity is zero and w is independent of x in the spanwise momentum equation, leading to the solution (21)). In addition, the real flow is turbulent, but the Reynolds stresses appearing in the spanwise momentum equation have been found to be several order of magnitude smaller than the rest of the terms (Ricco and Quadrio, 2008). We will come back to this in section 3.3 where the expression (21) is compared with the profiles taken from DNS. For now, we proceed with the analysis of (21) and subsequently compare the theoretical results with the full Navier-Stokes solution obtained numerically (DNS).

The spanwise velocity gradient at the wall can be calculated from (21) as,

$$w_y|_{y=0} = -W_m\sqrt{\omega/2\nu}\,[\cos(\omega t) + \sin(\omega t)] \tag{22}$$

However, since the wall starts oscillating from rest, a non-periodic solution containing also the transient behavior must be found. Kulish and Lage (2002) used fractional calculus to obtain such as a solution as

$$w_y|_{y=0} = -W_m\sqrt{\omega/\nu}\left[\sin(\omega t + \pi/4) - \sqrt{2}\Lambda\left(\sqrt{2\omega t/\pi}\right)\right] \tag{23}$$

where $\Lambda(z)$ is the auxiliary Fresnel function:

$$\Lambda(z) = [1/2 - C(z)]\cos\left(\frac{\pi}{2}z^2\right) + [1/2 - S(z)]\sin\left(\frac{\pi}{2}z^2\right) \tag{24}$$

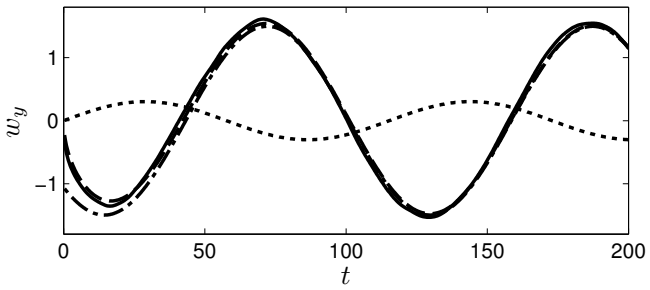

Figure 9: Development of the spanwise velocity gradient from the onset of oscillation. (—) DNS; (− −) Equation (23); (− · −) Equation (22); (· · ·) wall velocity. Results shown for case 1 at $x = 450$ and averaged over z.

In Equation (24) $C(z)$ and $S(z)$ refer to the Fresnel Integrals:

$$C(z) = \int_0^z \cos\left(\frac{\pi}{2}\xi^2\right) \mathrm{d}\xi \tag{25}$$

and

$$S(z) = \int_0^z \sin\left(\frac{\pi}{2}\xi^2\right) \mathrm{d}\xi \tag{26}$$

The resulting velocity gradient from DNS is compared with Equation (23) and Equation (22) in Figure 9. The simulation result taken from one streamwise position at $x = 450$ closely follows the non-periodic solution in the beginning of the oscillations. After only one period of oscillation the two theoretical solutions are indistinguishable and the DNS results follow the predicted values. Note that the velocity field is fully turbulent, but the spanwise shear follows the laminar solution nevertheless. A similar transient behavior was reported from channel flow DNS by Quadrio and Ricco (2003). However, in their case the spanwise shear was integrated over the surface of the whole computational box (both $x-$ and $z-$directions) whereas the present result is taken from a discrete point at $x = 450$ and averaged over z.

Figure 9 shows the results from case 1 but exactly the same curves are obtained from case 2 (and 3), albeit with a larger magnitude.

The reason behind the close agreement between DNS data and the laminar solution is further elaborated in section 3.3.

3.2.2. Streamwise shear

For the streamwise velocity gradient (which produces the viscous drag) there is no analytical solution. The flow is turbulent and hence the time-signal from a single streamwise position (although averaged over the spanwise direction) can be misleading. Therefore is an average value taken over the region downstream which exhibits a relatively constant DR; $x = 366 - 450$. The result is shown in Figure 10 as the solid line. A similar behavior of the streamwise shear as a function of the streamwise coordinate (x) can be observed from Figure 3 where

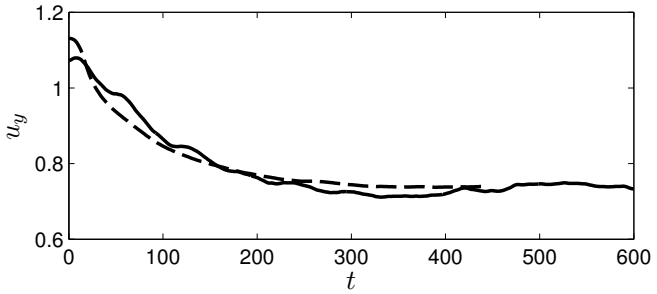

Figure 10: Development of the streamwise velocity gradient from the onset of oscillation. (—) Time-signal averaged over spanwise direction and over streamwise $x = 366$ to $x = 450$; (− −) Time-averaged and spanwise-averaged streamwise velocity gradient (with variation in x) with coordinate transformation according to $t = x/\mathcal{U}_w$. Results shown for case 2.

the statistically stationary flow data is used. (Note that the DR is essentially the streamwise shear.) Hence, a coordinate transformation between streamwise coordinate (x) and time (t) seems possible.

A convection velocity of the near-wall turbulence fluctuations (denoted $\mathcal{U}_w$) which relates the streamwise coordinate (x) and time (t) through $x = \mathcal{U}_w t$ is now introduced. An estimated value of $\mathcal{U}_w = 10u_\tau$ found in the literature (Kim and Hussain, 1993) is used. In the following the value of u_τ is taken from the reference case at the onset of oscillation, $u_\tau^0(x = 250)$. No difference in the results can be detected when using $u_\tau^0(x)$ instead, due to the moderate variation downstream.

Plotting the statistically stationary streamwise velocity gradient as a function of the transformed coordinate $t = x/\mathcal{U}_w$ (the dashed line in Figure 10) reveal the close relationship between the temporal transient in the spatially constant region and the spatial transient in the temporally constant regime. Note that the curve representing the stationary flow ends at $t = (470 - 250)/\mathcal{U}_w \approx 436$ since the oscillation starts at $x = 250$, and $x = 470$ is the last point for which we have fully turbulent flow.

Observe also that the spatial and temporal curves possess two different values of u_y at $t = 0$ due to that the time-signal is averaged over the streamwise direction ($x = 366 - 450$). When comparing with channel flow data, it may be surprising to note that the non-monotonic evolution in the streamwise shear observed by Quadrio and Ricco (2003) is not evident here.

3.2.3. Reynolds stresses

To further analyze the temporal and spatial transients we plot the longitudinal Reynolds stress (u_{rms}) at various representative $x-$positions (time averaged) and various time instances (averaged over $x = 366 - 450$) in Figure (11). All profiles are averaged over the homogeneous spanwise direction (z). The dashed line in Figure 11 is from time $t = 3/8\ T$ (averaged over $x = 366 - 450$) and the dashed line with symbols (◯) is the time averaged profile from $x = 3/8\ T\mathcal{U}_w$.

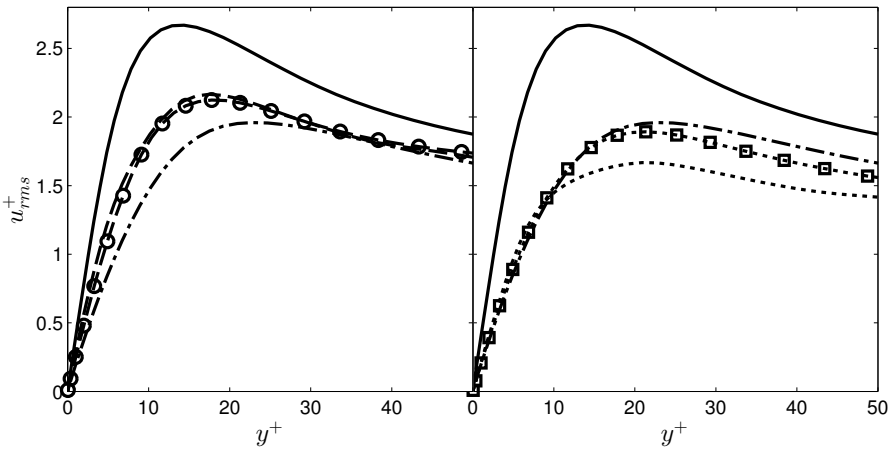

Figure 11: u_{rms} for case 2. $(-\ \cdot\ -)$ at $x = 450$ (long term statistics); (—) reference case. Left: $(-\ -)$ from $t = 3/8\ T$; $(-\ -\bigcirc)$ from $x = 3/8\ T\mathcal{U}_w$. Right: $(\cdots)$ from $t = T$; $(\cdots\ \square)$ from $x = T\mathcal{U}_w$.

The two profiles coincides for most of the inner part of the boundary layer and we can deduce that the coordinate transformation ($x = t\mathcal{U}_w$) maps the spatial evolution onto the temporal evolution. Furthermore, the profiles are located between the reference case (which may be interpreted as from time $t = 0$) and the long term statistics from the oscillating case (taken from $x = 450$), indicating that the flow is not yet (in time and downstream position respectively) adapted to the oscillating wall.

The agreement between profiles from a time t and profiles from a equivalent position $x = t\mathcal{U}_w$ is evident up to the time $t = 6/8\ T$ (not shown in Figure (11)). From this time and onward, the profiles from a time instance deviates from the ones taken from the corresponding $x-$positions. At the time $t = T$, the temporal profile, shown as the dotted line in Figure (11) is located below the long-term statistics, indicating a non-monotonic behavior, similar to what was observed in the channel flow simulations by Quadrio and Ricco (2003). The corresponding spatial profile taken from the long term statistics at $x = T\mathcal{U}_w$, which translates to $x = 308$, and shown as the dotted line with symbols ($\square$), deviates from the temporal profile but overlaps with the long-term statistics taken from $x = 450$. Thus, from the position $x = 308$ and onward, the u_{rms} profile has already reached the spatially independent profile even though the DR has yet to reach its constant value (see Figure 3).

As mentioned above, the non-monotonic temporal behavior observed in the channel flow simulations is also observed in the temporal boundary layer data, albeit the second extreme at $t = 6.6T$ observed in the channel flow, see (Quadrio and Ricco, 2003, Figure 10), is not present here (not shown in the figure).

For a clearer picture of the transients we plot the maximum value of u_{rms} (maximum taken in the $y-$direction) in Figure 12. The solid line represents the

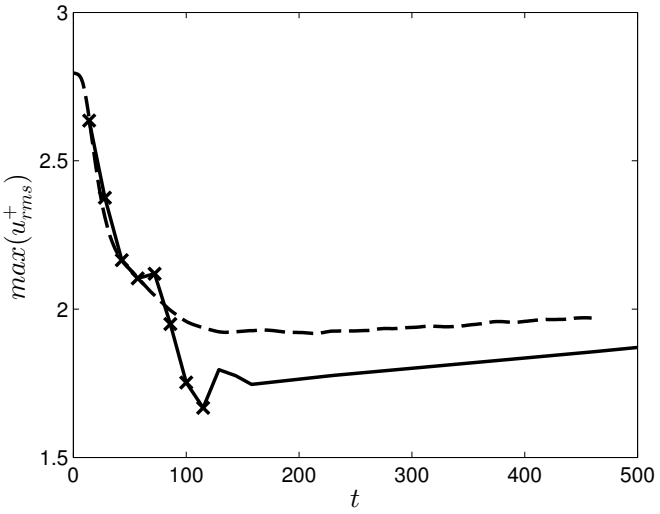

Figure 12: Maximum (over y) of u_{rms} for case 2. (—) Time-signal averaged over spanwise direction and over streamwise $x = 366$ to $x = 450$, symbols ($\times$) represent time instances one eighth of a period T (indicated only for the time $t = 0 - T$); ($- -$) Time-averaged and spanwise-averaged data (with variation in x) with coordinate transformation according to $t = x/\mathcal{U}_w$.

temporal signal while the dashed line indicates the spatial evolution (taken from time-averaged and spanwise-averaged data) with coordinate transformation according to $t = x/\mathcal{U}_w$. The symbols ($\times$) indicate the first period divided into eight segments. Hence the last symbol shows where the first period has been concluded. Here it is clearly illustrated that the transients follow each other until $t = 6/8\ T$, where the spatial transient levels off and the non-monotonic behavior in the temporal transient occurs. After reaching a minimum at $t = T$, the temporal profile relaxes slowly and approaches the long-term statistical value - which actually varies slowly downstream due to the (small) variation of Reynolds number and hence DR (cf. Figure 3).

By comparing the temporal and spatial transients we can now conclude that the temporal non-monotonic behavior has no correspondence in the spatial (downstream) development. However, before the u_{rms} profile reaches values below the the long-term statistics (at $t = 6/8\ T$), the coordinate transformation ($x = t\mathcal{U}_w$) does provide a mapping of the time-domain profile to the corresponding spatial profile.

In order to maximize the turbulence suppression, one might speculate that the transient effects could be utilized in some manner. Note however that, even though the turbulent fluctuations exhibit transients, the wall shear stress does not. Therefore it is an open question if exploiting the transients could be on any advantage for the purpose of maximizing the DR.

The behavior of the transients for the normal Reynolds stress (v_{rms}) is similar to the u_{rms}, except that the temporal profile reaches values below the long-

term statistics (the non-monotonic development) at a later time ($t = 2T$). This is in agreement with channel flow transients observed by Quadrio and Ricco (2003). When comparing various profiles from time t and long-term statistics from the corresponding spatial locations at $x = t\mathcal{U}_w$, the maximum of the spatial profiles are consistently about 10% lower than the maximum of the corresponding temporal profiles. Also the Reynolds shear stress exhibit the non-monotonic values at the later time as compared to the longitudinal Reynolds stress in agreement with Quadrio and Ricco (2003).

For the spanwise Reynolds stress (w_{rms}) the comparison between temporal and spatial transients cannot be made as the spatial curves are unobtainable due to the fact that the flow is non-homogeneous and time-dependent. However, the temporal profiles at various time instances can be obtained using the same methodology as above, i.e. by averaging over a region downstream which exhibits constant DR ($x = 366 - 450$), in order to compare with the channel flow transients in the investigation by Quadrio and Ricco (2003). The profiles up to time $t = T$ are shown in Figure 13 with the same symbols as in (Quadrio and Ricco, 2003, Figure 13). The simulation scaling has been retained in this plot (i.e. free-stream velocity U for w_{rms} and inlet displacement thickness δ^* for the vertical coordinate y). The profiles are very similar to the channel flow and the only noticeable difference is that the first peak in the profile from $t = 3/8\ T$ observed in channel flow data is not as developed in the present boundary layer data. Another minor difference is that the profile at $t = 6/8\ T$ is slightly lower in the present data. Otherwise the profiles are almost uncannily similar in channel and boundary layer flows. Specially important is the intense peak at $t = 4/8\ T$ and $t = 5/8\ T$ which is approximately 15% larger than the initial value (reference case) but is thereafter rapidly decreasing again, which in turn can be attributed to the rise and fall of the corresponding production term in the Reynolds stress budget equation.

Thus, the turbulence dynamics in the inner part of the boundary layer is similar to the channel flow and the conclusions regarding the mechanisms behind the DR drawn in Quadrio and Ricco (2003) and other publications (Choi et al., 2002; Xu and Huang, 2005, e.g.) can be imparted to the boundary layer flow.

In this section it has been shown that the temporal transients of Reynolds stresses in the boundary layer flow are similar to those in the channel flow. The profiles in the boundary layer case have been obtained by averaging in the spatial direction of constant DR. The spatial transients (at downstream positions before the DR is constant) have been shown to follow the temporal ones except for the non-monotonic behavior which is lacking in the spatial transients. The lack of non-monotonicity in the spatial transients of the turbulent fluctuations show that the evolution in time and space cannot be compared by using a single convective time scale, which on the other hand is possible for the streamwise shear.

To elucidate the differences between the temporal and spatial transients, all quantities influencing the Reynolds stress budget, and their spatial and temporal evolution, must be investigated. This is far too expensive with the current numerical tools and approach to turbulence statistics. Thus, new numerical

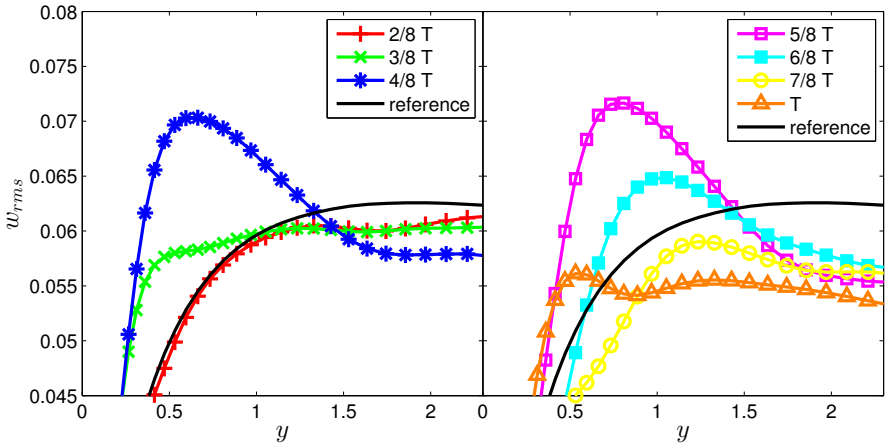

Figure 13: w_{rms} profiles for case 2 at time instances indicated in the legends. Colors in the electronic version follow the ones in (Quadrio and Ricco, 2003, Figure 13).

methods and a different kind of analysis may be required for a complete picture of the processes involved.

One possible reason for the differences between spatial and temporal transients is due to the evolution in time governed by the pressure-strain rate terms as shown by Xu and Huang (2005) for the parallel flow. Note that the spanwise Reynolds stress exhibits a maximum in their investigation, while no trough was detected in longitudinal, normal and shear Reynolds stresses, possibly due to the finite time intervals that their data were averaged over. Thus, our present data analysis demonstrates that great care has to be taken when investigating the turbulence statistics, otherwise important details may be obscured. As discussed above, in order to obtain a full picture of the transient behavior, all terms in the transport equations for the Reynolds stresses must be investigated. However, although a tedious exercise, the causality and physical understanding regarding the turbulence structures may still be elusive.

3.3. Instantaneous spanwise velocity profile

The profiles from Equation (21) is compared with the DNS data at four instances in time when the wall velocity is at its maximum and minimum levels, and zero respectively. The four curves are taken from time instances after the collection of statistics was performed and hence the flow has experienced a total number of 113 oscillations at this time. As the results in Figure 14 indicate, the overlap is very good. Thus, even in the boundary layer flow, where the flow is inhomogeneous in the downstream direction, the spanwise velocity profile follow the prediction derived from the laminar equations describing a parallel flow. For channel (Quadrio and Ricco, 2003; Choi et al., 2002) and pipe (Choi and Graham, 1998; Quadrio and Sibilla, 2000) flows, similar agreement between the laminar Stokes layer and instantaneous velocity profiles has been observed,

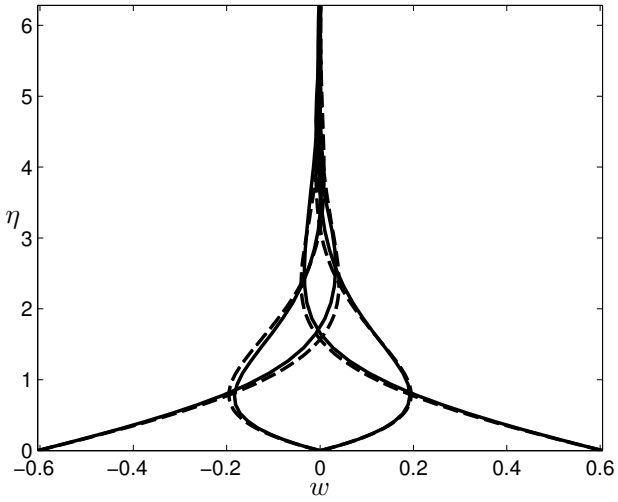

Figure 14: Spanwise velocity profiles from four points in time where the wall velocity is at its maximum and minimum levels, and zero respectively. (—) DNS; (− −) from Equation (21). Note that the average is only taken in the homogeneous spanwise direction. Results shown for case 2.

albeit in those cases the average has been taken in two homogeneous directions (x and z) while the present data in Figure 14 is only averaged in z.

The only previous attempt to show these profiles from a boundary layer are from the experimental study by Choi (2002). However, the profiles in this case were phase averaged and did not include the near-wall region.

The reason for the close similarity between the turbulent velocity field and laminar solution is that the Reynolds stress gradient terms in the spanwise momentum equation,

$$\frac{\partial}{\partial x}\overline{uw} \quad \text{and} \quad \frac{\partial}{\partial y}\overline{vw}$$

are several magnitudes lower than the rest of the terms, as shown by Ricco and Quadrio (2008). This is also the reason behind the agreement between the laminar solution and spanwise shear illustrated in Figure 9.

4. Conclusion

Direct Numerical Simulations have been performed to study the effect of wall oscillation with two different wall velocities but equal frequency on the turbulent boundary layer. The resulting drag reduction is 18% and 29% respectively, in agreement with findings from channel flow simulations, albeit slightly lower. The discrepancy in drag reduction can be attributed to either the different Reynolds number or geometry. Comparison with earlier channel flow simulations at various Reynolds numbers, and boundary layer experiments indicate that the former explanation is plausible.

A simulation with identical oscillation parameters as in earlier low Reynolds number channel flow and high Reynolds number boundary layer flow investigations confirm the variation of drag reduction with Reynolds number.

The Reynolds stresses are reduced by the oscillations and the effect on the maximum depends on whether the position of the maximum is inside or outside the laminar Stokes layer formed due to the oscillations.

An estimation of the idealized power consumption shows that a positive energy budget is only possible for the weaker wall velocity case. In the case of higher wall velocity more energy is required for the spatial oscillation than what is saved by drag reduction, although the drag reduction is enhanced compared to the weaker wall velocity case.

The time-signal of the spanwise shear from the onset of oscillations follows the non-harmonic solution to the laminar equations.

The close correspondence between the temporal and spatial transients through the coordinate transformation $t = x/\mathcal{U}_w$ has been demonstrated for the streamwise shear.

The spatial and temporal transients of the longitudinal Reynolds stress are very similar, albeit the non-monotonic development observed in the temporal transients are not detected in the spatial evolution of the flow. Furthermore, the spanwise Reynolds stress behaves almost exactly as in a channel flow.

Comparisons of the instantaneous spanwise velocity profiles with the analytical solution to the laminar Navier-Stokes equations show very good agreement.

5. Acknowledgments

Academic Research Fund Tier 1 (RG 37/10) from Ministry of Education, Singapore, is greatly acknowledged. Computer time from the High Performance Computing Centre at Nanyang Technological University was invaluable for the completion of the simulations.

References

Auteri, F., Baron, A., Belan, M., Campanardi, G., Quadrio, M., 2010. Experimental assessment of drag reduction by traveling waves in a turbulent pipe flow. Phys. Fluids 22 (115103).

Bandyopadhyay, P., 2006. Stokes mechanism of drag reduction. Journal of Applied Mechanics, Transactions ASME 73, 483–489.

Baron, A., Quadrio, M., 1996. Turbulent drag reduction by spanwise wall oscillations. Appl. Sci. Res. 55, 311–326.

Bradshaw, P., Pontikos, N., 1985. Measurements in the turbulent boundary layer on an 'infinite' swept wing. Journal of Fluid Mechanics 159, 105–130. Cited By (since 1996) 45.

Chevalier, M., Schlatter, P., Lundbladh, A., Henningson, D.S., 2007. SIMSON — A Pseudo-Spectral Solver for Incompressible Boundary Layer Flows. Technical Report. TRITA-MEK 2007:07. KTH Mechanics, Stockholm, Sweden.

Choi, J.I., Xu, C.X., Sung, H.J., 2002. Drag reduction by spanwise wall oscillation in wall-bounded turbulent flows. AIAA J. 40, 842–850.

Choi, K.S., 2002. Near-wall structure of turbulent boundary layer with spanwise-wall oscillation. Phys. Fluids 14, 2530–2542.

Choi, K.S., Clayton, B.R., 2001. The mechanism of turbulent drag reduction with wall oscillation. Intl J. Heat Fluid Flow 22, 1–9.

Choi, K.S., DeBisschop, J.R., Clayton, B.R., 1998. Turbulent boundary-layer control by means of spanwise wall oscillation. AIAA J. 36, 1157–1163.

Choi, K.S., Graham, M., 1998. Drag reduction of turbulent pipe flows by circular-wall oscillation. Phys. Fluids 10, 7–9.

Dhanak, M.R., Si, C., 1999. On reduction of turbulent wall friction through spanwise wall oscillations. J. Fluid Mech. 383, 175–195.

Di Cicca, G.M., Iuso, G., Spazzini, P.G., Onorato, M., 2002. Particle image velocimetry investigation of a turbulent boundary layer manipulated by spanwise wall oscillations. J. Fluid Mech. 467, 41–56.

Duggleby, A., Ball, K.S., Paul, M.R., 2007. The effect of spanwise wall oscillation on turbulent pipe flow structures resulting in drag reduction. Phys. Fluids 19 (125107).

Fang, J., Lu, L., 2010. Large eddy simulation of compressible turbulent channel flow with active spanwise wall fluctuations. Modern Physics Letters B 24, 1457–1460.

Jung, W.J., Mangiavacchi, N., Akhavan, R., 1992. Suppression of turbulence in wall-bounded flows by high-frequency spanwise oscillations. Phys. Fluids A 4, 1605–1607.

Karniadakis, G.E., Choi, K.S., 2003. Mechanisms on transverse motions in turbulent wall flows. Annu. Rev. Fluid Mech. 35, 45–62.

Kasagi, N., Suzuki, Y., Fukagata, K., 2009. Microelectromechanical systems-based feedback control of turbulence for skin friction reduction. Annu. Rev. Fluid Mech. 41, 231–251.

Kim, J., Hussain, F., 1993. Propagation velocity of perturbations in turbulent channel flow. Phys. Fluids A 5, 695–706.

Kulish, V., Lage, J., 2002. Application of fractional calculus to fluid mechanics. J. Fluids Eng. 124, 803–806.

Laadhari, F., Skandaji, L., Morel, R., 1994. Turbulence reduction in a boundary layer by a local spanwise oscillating surface. Phys. Fluids 6, 3218–3220.

Moin, P., Shih, T.H., Driver, D., Mansour, N., 1990. Direct numerical simulation of a three-dimensional turbulent boundary layer. Physics of Fluids A 2, 1846–1853.

Nikitin, N., 2000. On the mechanism of turbulence suppression by spanwise surface oscillations. Fluid Dynamics 35, 185–190.

Quadrio, M., Ricco, P., 2003. Initial response of a turbulent channel flow to spanwise oscillation of the walls. J. Turbul. 4, 7.

Quadrio, M., Ricco, P., 2004. Critical assessment of turbulent drag reduction through spanwise wall oscillations. J. Fluid Mech. 521, 251–271.

Quadrio, M., Ricco, P., 2011. The laminar generalized Stokes layer and turbulent drag reduction. J. Fluid Mech. 667, 135–157.

Quadrio, M., Ricco, P., Viotti, C., 2009. Streamwise-travelling waves of spanwise wall velocity for turbulent drag reduction. J. Fluid Mech. 627, 161–178.

Quadrio, M., Sibilla, S., 2000. Numerical simulation of turbulent flow in a pipe oscillating around its axis. J. Fluid Mech. 424, 217–241.

Ricco, P., 2004. Modification of near-wall turbulence due to spanwise wall oscillations. J. Turbul. 5, 24.

Ricco, P., Quadrio, M., 2008. Wall-oscillation conditions for drag reduction in turbulent channel flow. Intl J. Heat Fluid Flow 29, 601–612.

Ricco, P., Wu, S., 2004. On the effects of lateral wall oscillations on a turbulent boundary layer. Exp. Therm. Fluid Sci. 29, 41–52.

Schlatter, P., Orlu, R., 2010. Assessment of direct numerical simulation data of turbulent boundary layers. J. Fluid Mech. 659, 116–126.

Schlatter, P., Orlu, R., Li, Q., Brethouwer, G., Fransson, J.H.M., Johansson, A.V., Alfredsson, P.H., Henningson, D.S., 2009. Turbulent boundary layers up to re-theta=2500 studied through simulation and experiment. Phys. Fluids 21 (051702).

Schlichting, H., 1979. Boundary layer theory. McGraw-Hill. 7th edition.

Skote, M., 2011. Turbulent boundary layer flow subject to streamwise oscillation of spanwise wall-velocity. Phys. Fluids 23 (081703).

Trujillo, S.M., Bogard, D.G., Ball, K.S., 1997. Turbulent boundary layer drag reduction using an oscillating wall, in: AIAA Paper 97-1870, pp. 1–10. 4th AIAA Shear Flow Control Conf.

Viotti, C., Quadrio, M., Luchini, P., 2009. Streamwise oscillation of spanwise velocity at the wall of a channel for turbulent drag reduction. Phys. Fluids 21 (115109).

Xu, C.X., Huang, W.X., 2005. Transient response of reynolds stress transport to spanwise wall oscillation in a turbulent channel flow. Phys. Fluids 17 (018101).

Yudhistira, I., Skote, M., 2011. Direct numerical simulation of a turbulent boundary layer over an oscillating wall. J. Turbul. 12, 9.